Research Article ISSN 2771-666X

Journal of Advanced Materials Science and Engineering

Comparison of The Yield Strength of High-Entropy Solid Solutions Based on BCC and FCC Lattices Obtained in the Experiment and Calculation

Horban VF

M. Frantsevich Institute of Materials Science problems of the National Academy of Sciences of Ukraine, Kiev, Ukraine.

***Correspondence:**
Horban VF, M. Frantsevich Institute of Materials Science problems of the National Academy of Sciences of Ukraine, Kiev, Ukraine.

Received: 28 Oct 2024; **Accepted:** 25 Nov 2024; **Published:** 07 Dec 2024

Citation: Horban VF. Comparison of The Yield Strength of High-Entropy Solid Solutions Based on BCC and FCC Lattices Obtained in the Experiment and Calculation. J Adv Mater Sci Eng. 2024; 4(2): 1-5.

ABSTRACT

Based on the literature data, high-entropy alloys based on BCC or FCC phases were selected for which the ultimate strength from 214 to 2863 MPA was determined. Knowing the chemical composition of the selected high-entropy alloys, the average elastic modulus, distortion level, and mixing enthalpy were calculated. The use of formulas that use only their atomic radius and elastic modulus, mixing enthalpy to determine the theoretical level of hardness made it possible to establish the yield strength based on the ratio s0,2=0,3H.

Keywords

High-entropy alloys, BCC and FCC phase, Lattice parameter, Mixing enthalpy, Hardness, Elastic modulus, Distortion, Elastic limit, Plasticity.

Introduction

The conducted studies of high-entropy alloys (HEA) allowed us to establish the main features that contribute to their high physical and mechanical properties.

The main features affecting the physical and mechanical properties of wind farms include:

1. Increased entropy, which contributes to high thermal stability [1,2];
2. The electronic concentration determines the phase composition of HEA [3,4];
3. Distortion (lattice-distortion) is one of the main mechanisms of strengthening HEA [5,6];
4. Mixing Enthalpy- interaction forces between atoms, which affects the lattice parameter, elastic modulus and hardness [7,8];
5. The role of the most refractory element with this type of Lattice in the formation of the lattice parameter of a HEA [9,10].

To speed up the design of wind farms with pre-defined limits of strength, specific gravity, and operating temperature, computer modeling is used using such methods as CALPHAD, Phase field, Monte Carlo, and Molecular dynamics [11-13]. In [14], a formula for theoretical calculation of the hardness of HEA based on BCC or HCC phases is proposed. This article is devoted to the study of the yield strength of high-entropy solid solutions based on BCC and FCC lattices obtained in the experiment and calculated from hardness data, using only such constants of elements that were part of experimental alloys as atomic radius, elastic modulus and mixing enthalpy.

Material and Methodology

Using the mixture rule makes it possible to calculate the average values of the lattice radius (r_{mix}) and elastic modulus (E_{mix}) of selected compositions of high-entropy alloys.

The distortion (δ) was evaluated according to the formula:

$$\delta = \Sigma c_i |(r_i - r_{mix.})/r_{mix.}|) \quad (1)$$

where: c_i is the concentration of this kind of atoms, respectively, r_i is the atomic radius of the i atoms, r_{mix} is the average atomic radius of the alloy elements.

Table 1 shows the characteristics of the elements that were part of the studied solid-soluble wind farms and were used for calculations.

The value of the enthalpy of mixing was calculated as a linear combination of the interaction energies between pairs of atoms included in the alloy according to the formula:

$$\Delta H_{mix} = \sum_{i=1, j\neq i}^{n} 4H_{ij}^{mix} C_i C_j \quad (2)$$

where H_{ij}^{mix} is the enthalpy of mixing of two atoms i and j, calculated within the frame work of the Miedema model [15]. The data for the subsequent calculation are taken from [16].

In [14], taking Hooke's law as a basis, a formula for calculating hardness is proposed not based on the BCC or FCC of lattices, which showed a fairly high coincidence with experimental data. By setting the value of the theoretical hardness, it is possible to determine the elastic limit of a hard-soluble HEA. To determine the elastic limit for metals and alloys from the hardness data, the Tabor ratio is used - σ=H/3. When recalculating the yield strength of metals from the hardness data determined during microindentation, based on our own experimental data and literature [17, 18], the ratio $\sigma_{0,2}$=0,3H was chosen. The calculation of the yield strength of HEA based on the BCC or FCC phase was carried out by the formula:

$$\sigma_{0,2}=0,3(1-0,01\Delta H/kJ/mol)\bullet\delta\bullet E_{calcul} \quad (3)$$

where: ΔH is the mixing enthalpy value; δ is the distortion value; $E_{calcul.}$ - elastic modulus, which was determined by the formula:

$$E_{calcul}=E_{mix.}\,[1-\{K(r_{mix.}-r_{most\ refract.\ el.}/r_{most\ refract.\ el.})\}]\,\delta \quad (4)$$

where: $E_{mix.}$ - the modulus of elasticity of the composition is calculated according to the rule of the mixture, $r_{most\ refract.\ el.}$ - the radius of the most refractory element with a BCC or FCC lattice in the composition of the HEA, $r_{mix.}$.- the average radius of the composition is calculated according to the mixture rule; K is the coefficient. For BCC, it is 3,6; for FCC - 20.

Results and Discussion

Data on the chemical composition and yield strength of solid-soluble wind farms based on the BCC and FCC phases were taken from the literature sources [18-44]. (Table 2). In the future, using formulas (3, 4) and these elements (Table 1), which are part of HEA, calculations were made to determine the yield strength.

Table 1: Characteristics of the elements that make up the studied solid-soluble HEA.

	Al	Ti	Hf	Zr	Nb	V	Ta	Cr	Mo	W	Mn	Re	Fe	Co	Ni	Cu
r, nm	0,1427	0,1431	0,1577	0,1599	0,1426	0,1314	0,1429	0,1246	0,1362	0,1368	0,1350	0,1378	0,1241	0,1254	0,1245	0,1277
E, GPa	70	115	80	70	105	125	185	270	310	400	198	460	210	200	200	125

Table 2: Composition of solid-soluble HEA based on BCC and FCC phases and their calculated data for determining hardness and yield strength.

Alloys	$a_{mix,}$ нм	$E_{mix.,}$ GPa	$E_{cal.,}$ GPa	E/H x10^{-2}	δ, %	ΔH, kJ/mol	$H_{,(calaul)}$ GPa	$\sigma_{0,2,(calaul)}$ MPa	$\sigma_{0,2\ (ekcper.)}$ MPa	Ref.
$Al_{0.1}$CrNbVMo	0,1339	194	205,6	4,37	4,12	-5,9	9,00	2692	2863	19
W0.4(TaTiCrV)0.6	0,1360	260	265	3,60	3,53	-2,5	9,55	2876	2314	20
NbMoTaTi0.5Ni0.5	01388	188	206	3,20	3,2	-2,3	6,60	1980	1750	21
NbTaMoW	0,1396	250	228	2,33	2,20	-6,4	5,32	1593	1732	18
TiZrTaHfMo	0,1478	150	131	4,18	4,11	-1,8	5,48	1643	1600	22
TiZrTaNbMo	0,1449	155	147	4,36	4,13	-1,7	6,18	1854	1566	23
HfTaTiZrNbMo	0,1467	142	128	4,20	4,32	-1,4	5,59	1678	1512	21
$Mo_{31}Nb_{28}V_{31}Ti_{10}$	0,1371	174	169,6	3,17	3,09	-2,9	5,39	1617	1471	24
TiNbTaMoW	0,1402	221	203	2,26	2,15	-5,3	4,59	1378	1455	25
$Ti_{20}Zr_{20}Nb_{30}Mo_{30}$	0,1442	125	152	3,78	3,81	4,5	4,73	1421	1400	26
TiHfNbTaMo	0,1440	157	152	3,28	3,23	-1,4	4,99	1498	1369	21
TaNbVMoW	0,1379	225	218	1,93	1,88	-4,61	4,28	1286	1362	25
HfMoNbTiZr	0,1475	134	94	5,32	5,42	1,2	5,00	1450	1351	21
$Ti_{0,75}$NbMoTaW	0,1401	227	207	2,15	2,04	-5,5	4,46	1338	1304	27
TiZrTaNbMo	0,1449	155	147	4,29	4,13	-4,5	6,31	1297	1297	28
VTaNbMoW	0,1379	225	219	1,96	1,88	-4,6	4,31	1296	1246	23
$Ti_{30}V_{10}Hf_{20}Nb_{20}Ta_{10}Mo_7W_3$	0,1436	132	109	3,38	3,36	-0,7	3,69	1107	1225	29
TiNbMoTaW -	0,1403	221	200	2,27	2,16	-5,2	4,55	1362	1180	30
NbTaMoW	0,1396	250	233	1,84	1,73	-6.5	4,29	1287	1121	31
MoNbTaW	0,1379	225	218	1,83	1,87	0,06	4,04	1224	1058	23

Ti_2ZrVNb	0,1440	102	98	4,39	4,41	-0,01	4,30	1300	1058	32
$NbTiVTaAl_{0,5}$	0,1400	128	137,5	2,84	2,75	-3,2	3,90	1172	1012	33
$Ti_6Cr_{18,8}Fe_{18,8}Co_{28,2}Ni_{28,2}$	0,1258	205	163	1,95	1,65	-6,1	3,19	856	1000	34
$Ti_{37}V_{15}Nb_{22}Hf_{23}W_3$	0,1439	111	93,5	3,76	3,76	0,01	3,50	1054	977	35
$Ta_{0,19}Nb_{0,19}Hf_{0,2}Zr_{0,21}Ti_{0,21}$	0,1491	108	91	4,87	4,88	2,8	4,43	1330	929	36
$Ti_{0,38}Zr_{0,27}Nb_{0,26}Al_{0,036}V_{0,046}$	0,1469	95	84	4,98	4,76	-4,0	4,19	1257	806	37
$Ni_{0,33}Cr_{0,166}Co_{0,166}Fe_{0,25}W_{0,083}$	0,1256	227	186	1,55	1,50	-3,3	2,89	868	789	38
$Nb_{0,2}CrFe_{0,5}CoNi_{2,1}$	0,1254	207	179	1,27	1,19	-7,5	2,29	687	725	39
$CoCrCuFeNiAl_{0,5}$	0,1268	185	117	2,56	2,52	-4,8	3,08	926	707	40
CrFeMnCoNi	0,1267	211	136	1,61	1,66	-4,2	2,27	680	640	41
$Co_{40}Cr_{20}Ni_{15}Fe_{15}Mo_{10}$	0,1264	218	182	0,55	0.73	-3.5	1.37	412	423	42
$Co_{30}Cr_{25}Fe_{40}Ni_5$	0,1246	216	213	0,49	0,48	-2,5	1,05	315	400	43
CoCrFeNi	0,1247	215	214	0,31	0,30	-2,0	0,65	215	214	44

The calculations performed showed that the obtained values of the yield strength coincide quite well with those obtained in the experiment for solid-soluble wind farms based on both the BCC and FCC phases (Figure 1). However, it should be noted that at high values of the calculated yield strength, the differences to the experimental values increase. This can be explained by the fact that these theoretical calculations do not take into account the defect rate of cast alloys. Also, the decrease in the yield strength is affected by the presence of a dendrites structure with different chemical compositions in cast wind farms. Conducting multi-hour annealing helps to equalize the chemical composition of cast HEA and increase the yield strength [45].

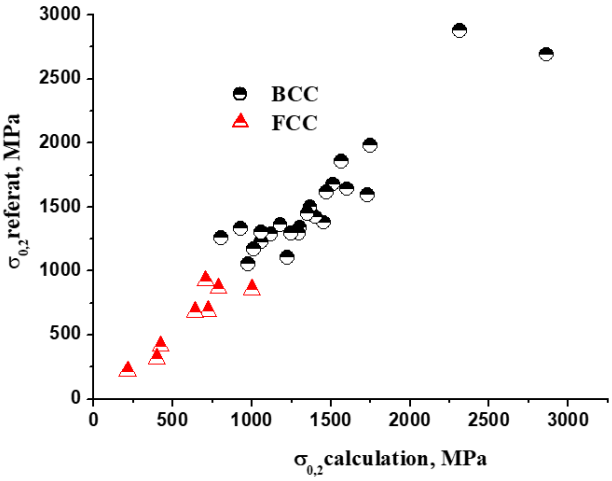

Figure 1: Comparative characteristics of the calculated yield strength with those obtained in the experiment for solid-soluble HEA based on BCC and FCC phases.

In [46], it is shown that for all materials there is a direct proportional dependence of the normalized hardness on elastic deformation. A similar proportional relationship was found for such indicators of high-entropy alloys as distortion and elastic deformation [14]. Indeed, if we determine the level of normalized hardness based on the calculated hardness and elastic modulus, then there is a direct proportional relationship between the calculated normalized hardness and distortion (Figure 2). This once again confirms the correctness of the chosen approach to calculating hardness, elastic modulus, and yield strength.

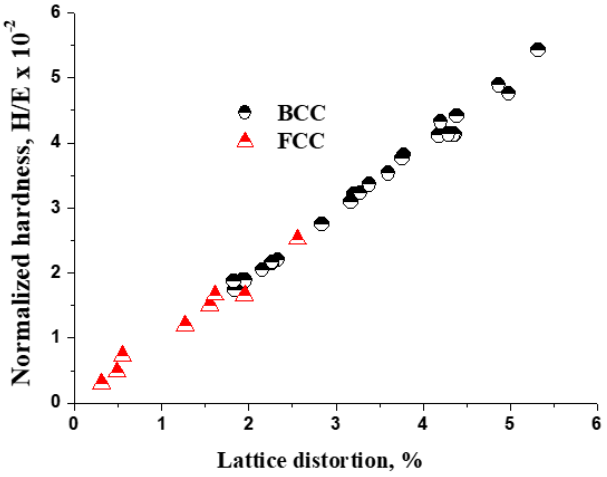

Figure 2: The relationship between the normalized hardness determined by the calculated hardness and elastic modulus indicators and the distortion.

Conclusion

The possibility of preliminary calculation of the elastic limit of hard-soluble high-entropy alloys based on BCC and FCC phases using only their atomic radius, elastic modulus, distortion, and mixing enthalpy is shown. A direct proportional relationship is revealed between the ratio of the calculated hardness to the calculated elastic modulus (normalized hardness) and distortion in solid-soluble HEA based on the BCC and FCC phases.

References

1. Murty BS, Yeh JW, Ranganathan SPP. Bhattacharjee High-Entropy Alloys. Second Edition. 2019; 363.
2. George EP, Curtin WA, Tasan CC. High entropy alloys: A focused review of mechanical properties and deformation mechanisms. Acta Materialia. 2019; 78: 435-474.
3. Zhang Y, Zhou YJ. Solid solution formation criteria for high entropy alloys. Mater Sci Forum. 2007; 561-565: 1337-1339.

4. Firstov SA, Gorban VF, Krapivka NA, et al. Structural materials research: Effect of electron density on phase composition of high-entropy equiatomic alloys. Powder Metallurgy and Metal Ceramics. 2016; 54: 607-613.
5. Wang Z, Fang Q, Li J, et al. Effect of lattice distortion on solid solution strengthening of BCC high-entropy alloys. J Mater Sci Technol. 2018; 34: 349-354.
6. Gorban VF, Firstov SO, Krapivka MO. Influence of various factors on the properties of solid-soluble high-entropy alloys based on BCC and FCC phases. Materials Science. 2022; 58. 135-140.
7. Otto F, Yang Y, Bei H, et al. Relative effects of enthalpy and entropy on the phase stability of equiatomic high entropy alloys. Acta Mater. 2013; 61: 2628-2638.
8. Gorban VF, Krapivka NA, Firstov SA, et al. The role of mixing enthalpy in the formation of physicomechanical properties of solid solution highly entropic alloys. Kiev IPMS. 2019; 12: 8-16.
9. Firstov SA, Mileyko ST, Gorban VF, et al. Modulus of elasticity of high-entropy single-phase alloys with a BCC crystal lattice. Composites and Nanomaterials. 2014; 1: 3-17.
10. Gorban VF, Krapivka NA, Firstov SA. High-entropy alloys: Interrelations between electron concentration, phase composition, lattice parameter, and properties. Physics of Metals and Metallography. 2017; 118: 970-981.
11. Kim G, Diao H, Lee C, et al. First-principles and machine learning predictions of elasticity in severely lattice-distorted high-entropy alloys with experimental validation. Acta Mater. 2019; 181: 124-138.
12. Li Y, Guo W. Machine-learning model for predicting phase formations of high-entropy alloys. Physical Review Materials. 2019; 3: 095005.
13. Del Grosso MF, Bozzolo G, Mosca HO. Modeling of high entropy alloys of refractory elements. Phys B: Condensed Matter. 2012; 407: 3285-3287.
14. Horban VF. Dising of solid solution high entropy alloys with BCC of FCC crystal structures. J of Mater Eng. 2024; 52: 16-26.
15. Miedema AR, de Chatel PF, de Boer FR. Cohesion in alloys – fundamentals of a semi-empirical model. Physica B+C. 1980; 100: 1-28.
16. http://www.entall.imim.pl/calculator/.
17. Gorban VF, Krapivka MO. Properties of cast multicomponent high-entropy boron-doped alloys. SCIREA J of Mater. 2024; 9: 13-21.
18. Xu C, Fang L, Xu G, et al. Mechanical properties and oxidation behavior of NbMoTaWx refractory high entropy alloys. J of Alloys and Compd. 2024; 990: 174390.
19. Kang B, Lee J, Ryu HJ, et al. Microstructure, mechanical property and Hall-Petch relationship of a light-weight refractory Al 0.1CrNbVMo high entropy alloy fabricated by powder metallurgical process. J Alloy and Compd. 2018; 767: 1012-1021.
20. Xiang C, Han EH, Zhang Z, et al. Microstructure, Mechanical Properties and Corrosion Resistance of the Mo05V05NbTiZrx High-Entropy Alloys with Low Thermal Neutron Sections. Acta Metallurgica Sinica (English Letters). 2024; 37: 1643-1656.
21. Tseng KK, Juan CC, Tso S, et al. Effects of Mo, Nb, Ta, Ti, and Zr on mechanical properties of equiatomic Hf-Mo-Nb-Ta-Ti-Zr alloys. Entropy. 2018; 21: 15.
22. Senkov ON, Gorsse S, Miracle DB, et al. Correlations to improve high-temperature strength and room temperature ductility of refractory complex concentrated alloys. Materials & Design. 2024; 239: 112762.
23. Shen X, Guo Z, Liu F, et al. Microstructural evolution and mechanical behavior of novel TiZrTaxNbMo refractory high-entropy alloys. J of Alloys and Compd. 2024; 990: 174459.
24. Regenberh M, Hasenmann G, Wilke M, et al. Microstructure evolution and mechanical properties of refractory Mo-Nb-V-W-Ti high entropy alloys. Metals. 2020; 10: 1530.
25. Han ZD, Luan HW, Liu X, et al. Microstructures and mechanical properties of TixNbMoTaW refractory high-entropy alloys. Mater Sci Eng: A. 2018; 712: 380-385.
26. Couzinié JP, Senkov ON, Miracle DB, et al. Comprehensive data compilation on the mechanical properties of refractory high-entropy alloys. Data Brief. 2018; 21: 1622-1641.
27. Han ZD, Luan HW, Liu X, et al. Microstructures and mechanical properties of Tix NbMoTaW refractory high-entropy alloys. Mater Sci Eng: A. 2018; 712: 380-385.
28. Shen X, Guo Z, Liu F, et al. Microstructural evolution and mechanical behavior of novel TiZrTaxNbMo refractory high-entropy alloys. J of Alloys and Compd. 2024; 990: 174459.
29. Wei QI, Zhang A, Han J, et al. Development of a Ti30Hf20Nb20Ta10V10Mo7W3 refractory high entropy alloy with excellent mechanical properties and wear resistance. J of Alloys and Compd. 2023; 966: 171571.
30. Kim YS, Ozasa R, Sato K, et al. Design and development of a novel non-equiatomic Ti-Nb-Mo-Ta-W refractory high entropy alloy with a single-phase body-centered cubic structure. Scripta Materialia. 2024; 252: 116260.
31. Zhang J, Hu Y, Wei Q, et al. Microstructure and mechanical properties of RexNbMoTaW high-entropy alloys prepared by arc melting using metal powders. J Alloy Compd. 2020; 827: 154301.
32. Huang T, Wu S, Jiang H, et al. Effect of Ti content on microstructure and properties of TixZrVNb refractoryhigh-entropy alloys. Intern J of Mine Metal and Mater. 2020; 27: 1318-1325.
33. Yang X, Zhang Y, Liaw PK. Microstructure and compressive properties of NbTiVTaAlx high entropy alloys. Procedia Eng. 2012; 36: 292-298.
34. Manzoni AM, Haas S, Daoud H, et al. Tensile Behavior and Evolution of the Phases in the Al10Co25Cr8Fe15Ni36Ti6 Compositionally Complex/High Entropy Alloy. Entropy. 2018; 20: e20090646.

35. Huang W, Wang X, Qiao J, et al. Edge dislocation-induced high-temperature strengthening in the Ti37V15Nb22Hf23W3 refractory high-entropy alloys. Mater Sci and Eng: A. 2024; 902: 146634.

36. Senkov ON, Scott JM, Senkova SV, et al. Woodward, Microstructure and elevated temperature properties of a refractory TaNbHfZrTi alloy. J Mater Sci. 2012; 47: 4062-4074.

37. Wang H, Chen W, Fu Z, et al. Lightweight Ti-Zr-Nb-Al-V refractory high-entropy alloys with superior strength-ductility synergy and corrosion resistance. Intern J of Refrac Meta and Hard Mater. 2023; 116: 106331.

38. Gu Z, He J, Qin Y, et al. Ultra strong FCC structured Ni8Cr4Co4Fe6W2 high entropy alloys with high strength and ductility by laser powder bed fusion. J of Alloys and Compd. 2024; 992: 174580.

39. Wang F, Guo Y, Liu Q, et al. A novel D022 precipitation-hardened Ni2.1CoCrFe0.5Nb0.2 high entropy alloy with outstanding tensile properties by additive manufacturing. Virtual and Physical Prototyping. 2023; 18: e2147553.

40. Wang FJ, Zhang Y, Chen GL, et al. Tensile and compressive mechanical behavior of a CoCrCuFeNiAl0.5 high entropy alloy. Int J Mod Phys. 2009; 23: 1254-1259.

41. Otto F, Dlouhy A, Somsen CH, et al. The influences of temperature and microstructure on the tensile properties of a CoCrFeMnNi high-entropy alloy. Acta Mater. 2013; 61: 5743-e5755.

42. Lee M, Choi G, Lee K. TRIP behavior of non-equiatomic Co40Cr20Ni15Fe15Mo10 high entropy alloys. Interna J of Refra Metals and Hard Mater. 2023; 115: 106288.

43. Chen W, Li B, Yang H, et al. Efect of B contention microstructure and mechanical properties of (Co30Cr25Fe40Ni5)100 xBx high entropy alloys. J of Mater Rese. 2023; 38: 3187-3198.

44. Li C, Sun Z, Xu Z, et al. Microstructure and Mechanical Properties of In Situ Self-generated VC Reinforced CoCrFeNi High-Entropy Alloy. J of Mater Eng and Performance. 2024; 33: 6237-6248.

45. Li J, Lu Y, Dong Y, et al. Annealing effects on the microstructure and properties of high-entropy CoCrFeNiTi0.5 alloy casting ingot. Ibid. 2014; 44: 37-43.

46. Gorban VF, Pechkovskii EP. Instrumented indentation for determining the structural state of materials. Powder Metallurgy and Metal Ceramics. 2010; 49: 424-429.